ADVANCED HEALTHCARE MATERIALS
www.advhealthmat.de

Experimental Study on Repairing Peripheral Nerve Defects with Novel Bionic Tissue Engineering

Tong Qi, Xu Zhang, Xiaosong Gu, and Shusen Cui**

Peripheral nerve defects are a worldwide problem, and autologous nerve transplantation is currently the gold-standard treatment for them. Tissue-engineered nerve (TEN) grafts are widely considered promising methods for the same, and have attracted much attention. To improve repair, the incorporation of bionics into TEN grafts has become a focus of research. In this study, a novel bionic TEN graft with a biomimetic structure and composition is designed. For this purpose, a chitin helical scaffold is fabricated by means of mold casting and acetylation using chitosan as the raw material, following which a fibrous membrane is electrospun on the outer layer of the chitin scaffold. The lumen of the structure is filled with human bone mesenchymal stem cell-derived extracellular matrix and fibers to provide nutrition and topographic guidance, respectively. The prepared TEN graft is then transplanted to bridge 10 mm sciatic nerve defects in rats. Morphological and functional examination shows that the repair effects of the TEN grafts and autografts are similar. The bionic TEN graft described in this study shows great potential for application and offers a new way to repair clinical peripheral nerve defects.

1. Introduction

The high disability rate caused by peripheral nerve injury is a serious clinical problem, and the main therapy for it is tension-free suturing of proximal and distal nerve residues.[1] High tension makes nerve sutures ineffective when the peripheral nerve defect affects a large area, potentially causing even more damage.[2] Under these circumstances, the alternative treatment is autologous nerve transplantation.[3] However, tumor growth, donor shortage, and other factors seriously hinder the practical application of the same.[4–6] Of late, bionic tissue-engineered nerve (TEN) grafts are being increasing investigated, because of their better repair efficiency,[7–10] with structural and component bionics being the key research foci.

Most TEN grafts are constructed based on nerve scaffolds, to provide physical and nutritional support for repairing nerve injuries.[11,12] In the past decade, structural biology has helped make vast improvements over the simple hollow tubes that were used previously as neural scaffolds, and allowed the use of more complex shapes that are more similar to the macro- and microstructures of peripheral nerves.[13–16]

Chitosan, a promising biomaterial, has been widely studied and applied as a nerve scaffold.[17] It has good biocompatibility and can support axonal regeneration, as well as reduce the amount of scar tissue.[18–23] In addition, its polysaccharide structure and physiological characteristics allow for its safe biodegradation, without negative effects or toxic metabolites. In addition, its degradation products, chitosan oligosaccharides, also play an active role in nerve regeneration.[18,23,24] However, the degradability of chitosan, especially that of low-acetyl chitosan, is insufficient. Generally, the higher the degree of acetylation, the better is the degradability. When the degree of acetylation is greater than 50%, chitosan is converted into chitin.[25–27] Considering the poor processability of chitin,[28] acetylation of chitosan scaffolds is a feasible solution for fabricating chitin scaffolds.[29,18]

It has been shown that cylindrical scaffolds prepared by freeze-drying after casting exhibit poor permeability. The material obtained by means of electrospinning exhibits good permeability, but has poor mechanical properties.[30] Therefore, in the present study, a combination of the two was used to create a helical-shaped freeze-dried scaffold with an electrospun outer scaffold layer, to improve permeability. This is a novel structural

T. Qi, S. Cui
Department of Hand Surgery
China-Japan Union Hospital
Jilin University
Changchun 130033, China
E-mail: sscui916@126.com
X. Zhang, X. Gu
Key Laboratory of Neuroregeneration of Jiangsu and Ministry of Education
Co-innovation Center of Neuroregeneration
NMPA Key Lab for Research and Evaluation of Tissue Engineering Technology Products
Nantong University
Nantong 226000, China
E-mail: nervegu@ntu.edu.cn

The ORCID identification number(s) for the author(s) of this article can be found under https://doi.org/10.1002/adhm.202203199

DOI: 10.1002/adhm.202203199

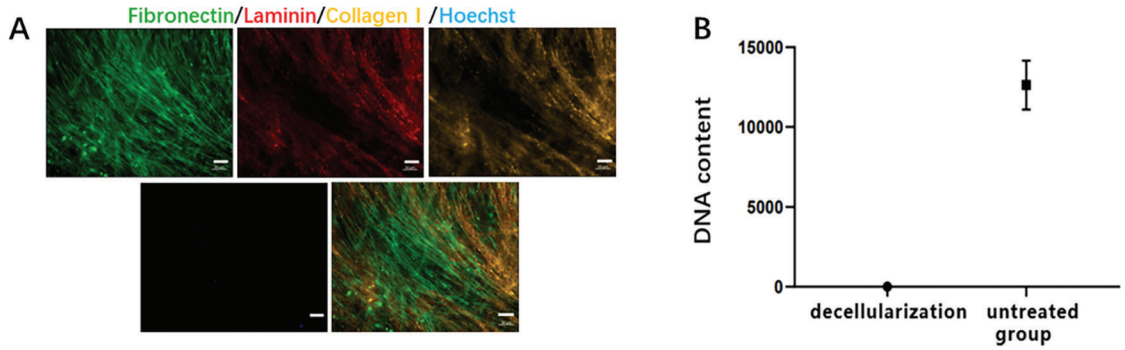

Figure 1. A) Immunochemistry micrographs showed that fibronectin (green), laminin (red), and collagen I (yellow) were expressed in the hBMSC-dECM; Scale bar: 50 μm. B) Comparing DNA content between untreated hBMSCs and cultured hBMSC-dECM. Data presented as mean ± SD, $n = 6$.

design that is conducive to the exchange of matter and reduces the amount of raw materials needed, thereby making stents lighter and thinner and reducing the risk of possible foreign body reactions.

The extracellular matrix (ECM) is a natural matrix that provides supporting structures and attachment sites for cells.[31] ECM also produces biological signaling molecules that are important for the construction and maintenance of the active tissue regeneration microenvironment.[32,33] Compared to ECM from tissues, ECM from cells is easier to obtain.[34] In addition, the ECM from cells can be better modified and transplanted to the surface of other biomaterials, simulate peripheral nerve ECM, and provide a microenvironment for axon regeneration to improve the function of TEN grafts. Our team compared many different cellular sources of ECM and found that bone mesenchymal stem cell-derived ECM (BMSC-dECM) can better simulate the inherent biochemical and mechanical signals of natural nerve ECM, thereby producing a harder and more stable structure than that of ECM from other cellular sources. In addition, the protein composition of BMSC-dECM is more similar to that of autogenous nerves, and can provide a large number of rich protein components instead of seed cells, which makes it an ideal ECM source for component bionics.[35] Therefore, in this study, we used human BMSC-dECM (hBMSC-dECM) to fill and modify nerve scaffolds.

Previously, nerve scaffolds in the form of simple tubes for proximal and distal nerve stumps were used to repair short-distance (<5 mm) defects.[36–38] However, for longer regeneration distances, intraluminal microstructures are indispensable for effective axonal guidance.[39,40] After a peripheral nerve injury, most chemical guidance clues secreted by axons are absent and may cause serious consequences or even produce neuromas.[41–43] Similar to other cell types, growing neuronal axons can sense and grow in the direction of topographic guidance in their environment, and increasing terrain can promote the growth of regenerative axons.[44,42,45] Topographic guidance commonly used for TEN grafts includes microchannels of the inner wall of nerve scaffolds and inner nanofiber scaffolds.[46–51] Many studies have shown that the high specific surface area of the inner fiber can provide more opportunities for cells to communicate with the surrounding environment and promote cell adhesion and proliferation.[52–55] The addition of growth factors can improve the affinity of the inner fibers to cells, thereby improving the repair efficiency.[55] Therefore, we designed fibers with a special T-shaped section using a mixture of chitosan and hBMSC-dECM, and placed it in the center of the nerve scaffold, to guide the topography of axon regeneration and further realize structural bionics.

In this study, we used chitin, the acetylated product of chitosan, to create nerve scaffolds with an electrospun outer layer, and hBMSC-dECM and chitosan to make the inner fibers, which were filled with hBMSC-dECM, as a stable source of nutritional factors. This resulted in a novel bionic TEN graft that exhibited similar results to those of autografts in repairing 10-mm sciatic defects in rats. This study presents an unusual method for synthesizing and constructing novel bionic TEN grafts, thereby laying the foundation for optimizing the clinical therapy of peripheral nerve defects.

2. Results

2.1. Characterization of hBMSC-dECM

To verify the main components and acellular effects of hBMSC-dECM, immunohistochemistry was used to confirm that hBMSC-dECM contained three main glycoproteins: fibronectin, laminin, and collagen I, which promote nerve regeneration.[56] Immunohistochemistry analysis showed no Hoechst labeling, indicating that the cellular components were almost completely removed from the ECM (**Figure 1**A). The results of DNA content detection also demonstrated that compared to that in the untreated cells, the DNA content was almost undetectable in the components that had undergone a complete decellularization step (Figure 1B).

2.2. TEN Graft Characterization

The Fourier transform infrared (FTIR) spectra showed that before acetylation (red), 1417 cm^{-1} corresponded to the tensile vibration of -NH in chitosan, while after acetylation (blue), there was an absorption peak at 3268 cm^{-1}, corresponding to the -$NHCOCH_3$ groups, and also at 1636 and 1547 cm^{-1}, corresponding to the shear vibrations of amide bonds (**Figure 2**A). Using Stephan's method for analysis and calculations,[57] the degree of acetylation in the sample was 4.73% before acetylation

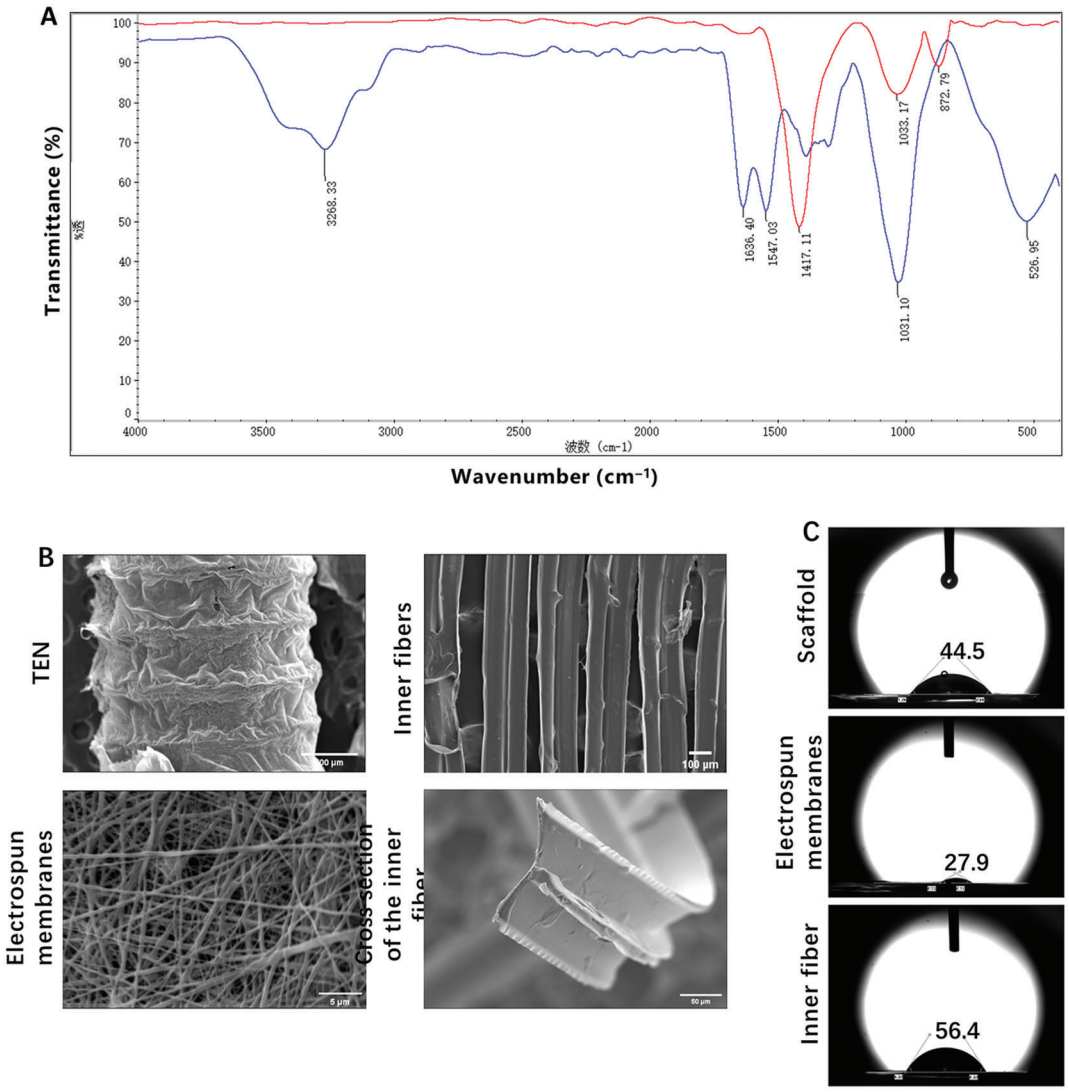

Figure 2. A) FTIR spectra of the scaffold before (red) and after (blue) acetylation. B) SEM images of the outermost electrospun membranes and inner fibers. C) Water contact angle of each layered structure of the TEN graft.

and 74.77% after acetylation. It can thus be concluded that chitosan was present before acetylation, while chitin was produced by acetylation. Scanning electron microscopy (SEM) analysis showed that the average pore size of the outermost electrospun chitosan membrane was $0.469 \pm 0.083\ \mu m^2$, while the diameter of the inner fibers was $181.497 \pm 8.499\ \mu m$. The cross-section of the fiber clearly showed a T-shape, consistent with the shape of the designed polydimethylsiloxane mold, which was conducive to cell adhesion and migration (Figure 2B). The results showed that the water contact angle (WCA) of all components in the TEN graft was less than 90°, indicating hydrophilicity (Figure 2C).

2.3. Cytotoxicity and Biocompatibility

The effect of the TEN graft on cell activity was detected using 3-(4,5-dimethylthiazol-2-yl)-2,5-diphenyltetrazolium bromide (MTT) assay, in which the optical density of the samples was measured to determine cell viability. The cell survival rates of the TEN graft-incubated samples confirmed that the TEN graft was nontoxic to L929 cells (**Figure 3**A).

Hemolysis testing was also performed to determine the blood compatibility of the TEN graft materials. The hemolysis rate of the TEN graft materials was 2.15%, which is within the recommended ISO standard 10993–4 of less than 5% for hemolysis of blood contact materials, thereby indicating good blood compatibility. The results of cytotoxicity and hemolysis tests showed that the TEN graft materials met the basic conditions for in vivo implantation.

2.4. In Vitro and In Vivo Degradation

An in vitro degradation test showed that the acetylated chitin and chitosan samples displayed a difference in their degradation rates. The high degradation rate of chitosan may be due to its

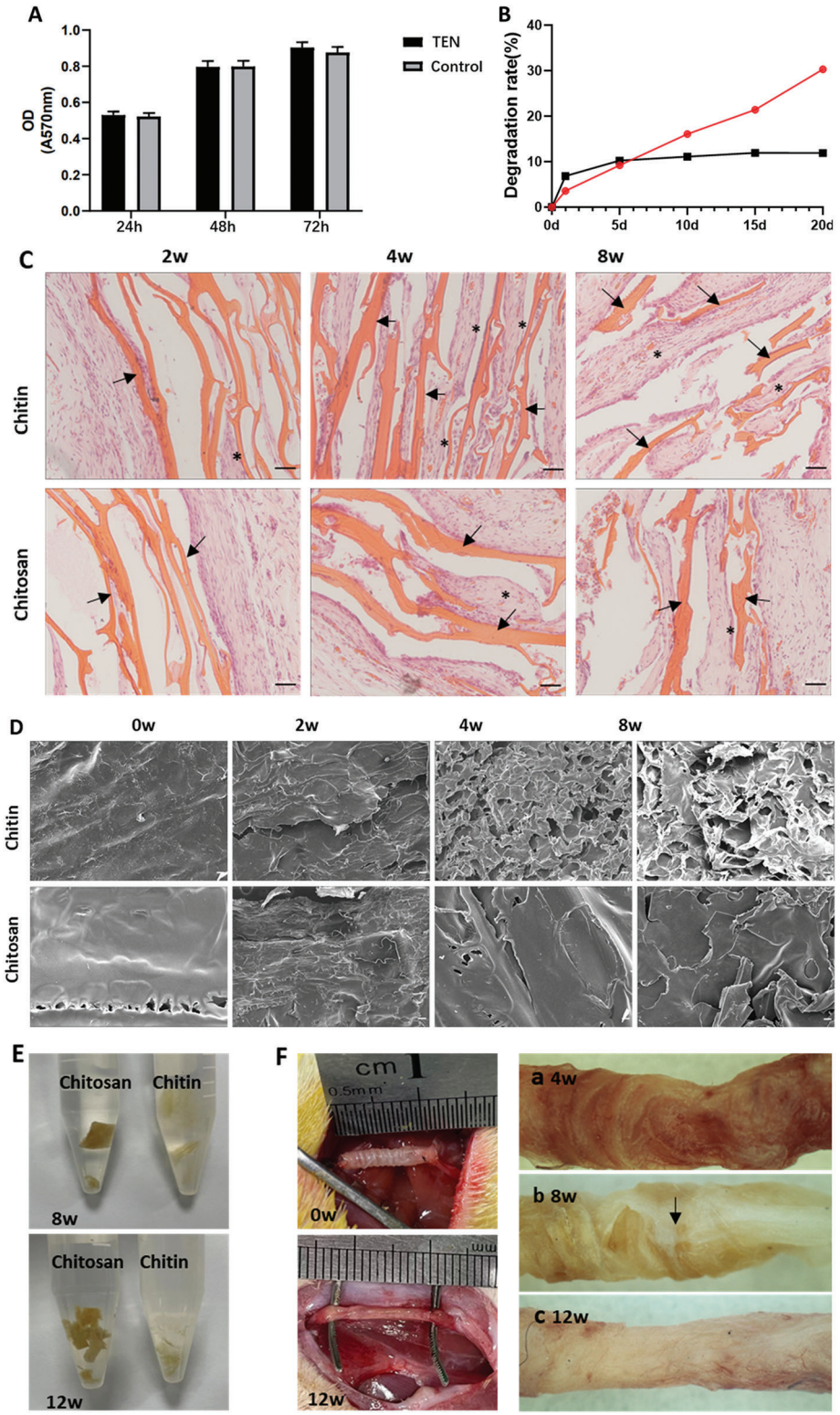

Figure 3. A) Optical densities of L929 cells incubated in extracts obtained from the TEN grafts, for 24, 48, and 72 h. Data presented as mean ± SD, $n = 6$. B) In vitro degradation of chitin (red) and chitosan (black). C) Hematoxylin and eosin staining of subcutaneously implanted pieces and surrounding tissue; samples have been indicated using arrows; invaded tissue has been marked using asterisks; Scale bar: 50 µm. D) SEM images of the removed tissue samples; Scale bar: 50 µm. E) Surrounding tissue from the removed subcutaneously implanted pieces; F) The exterior of the TEN graft at the time of surgery (0 w), and at 4, 8, and 12 weeks post-operation.

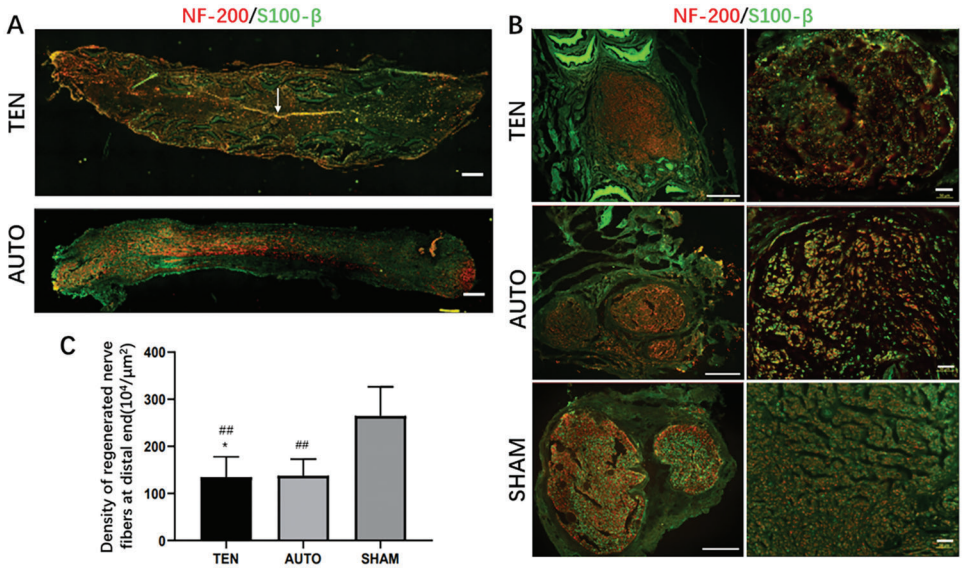

Figure 4. A) NF200 (red) and S100β (green) immunolabeling of longitudinal sections of regenerated nerves harvested after 3 weeks, with the inner fiber indicated using arrows; scale bar: 500 μm. B) Immunohistochemistry of the regenerated nerves in the three groups carried out using anti-NF200 (red) and anti-S100β (green) antibodies at 8 weeks post-surgery; scale bars: 500 μm (left) and 50 μm (right). C) Histogram of the number of NF200-positive fibers in distal samples in the three groups. Data are expressed as mean ± SD, $n = 15$, one-way ANOVA was carried out across groups, *n.s. versus AUTO group and ##$p < 0.01$ versus SHAM group.

partial dissolution in phosphate-buffered saline. Chitosan almost completely stopped degrading after 5 d, while the degradation rate of chitin increased. At 20 d, the degradation rate of chitin exceeded 30%, whereas that of chitosan remained stable at 10% (Figure 3B).

Hematoxylin and eosin (H&E) staining analysis showed that the chitosan samples maintained their shape and thickness at 4 weeks, were slightly broken at 8 weeks, and at 12 weeks, showed debris and tissue invasion, which was more obvious than those at 4 weeks. After 8 weeks, the chitin samples were completely broken into pieces. In addition, none of the samples exhibited obvious inflammatory responses (Figure 3C).

After removing the surrounding tissue, SEM analysis showed that the chitin samples began to crack at 2 weeks, and as time progressed, the fragmentation changed significantly at 4 weeks, whereas the chitosan samples began to crack after 8 weeks without fragmentation (Figure 3D). It could be observed with the naked eye that the chitosan samples remained intact after being embedded subcutaneously onto the backs of rats for 8 weeks, and were broken but showed no significant changes in thickness at 12 weeks. The acetylated chitin samples were degraded into thin films after 8 weeks, and degraded into fragments at 12 weeks (Figure 3E).

2.5. Post-Surgery Observations

After the surgery, there was no inflammation in the surgical area, and no obvious abnormalities were observed in the TEN, SHAM, and AUTO groups. Foot swelling and toe ulcerations were observed on the operative side in the NON group. After surgery, when the muscle gap was opened to remove the bridging segmental nerve, it was observed that there were no obvious inflammatory reactions, such as adhesion, swelling, or bleeding in the surrounding tissue. At 4 weeks, the TEN graft structure was still clearly visible; at 8 weeks, part of the TEN graft structure was visible, and part of the material was degraded, exposing the inner new nerves (indicated using arrows); and at 12 weeks, the TEN graft structure was no longer visible, and the scaffold was almost completely degraded, with only new nerves observed (Figure 3F).

2.6. Morphological Evaluation of Regenerated Nerves

3 weeks after the surgery, axonal regeneration was observed using anti-NF200 and anti-S100β immunohistochemical staining (**Figure 4**A). The regenerated axons in the TEN graft extended from proximal to distal along the guiding fibers (arrow in Figure 4A), along a straight path with multiple branches.

Regenerated axons extending distally were detected using anti-NF200 and anti-S100β immunofluorescence double staining at 8 weeks post-operation (Figure 4B). Upon quantitative comparison, the density of regenerated axons between the TEN and AUTO groups was not statistically different, but obviously different from that of the SHAM group (Figure 4C).

Myelinated nerve fibers that regenerated distally from the injury were observed using transmission electron microscopy (TEM) at 12 weeks post-operation (**Figure 5**A). The myelin sheath thicknesses in the TEN, AUTO, and SHAM groups were 556.153 ± 44.854, 564.587 ± 38.925, and 1115.174 ± 23.658 nm, respectively, while the myelin layers were 49.878 ± 8.579, 45.098 ± 8.015, and 89.19 ± 11.229, respectively. The TEN and AUTO groups had similar myelin thickness and layers (Figure 5B), which suggested that the effects of the bionic TEN grafts on promoting peripheral nerve regeneration were similar to those of the autogenous nerves.

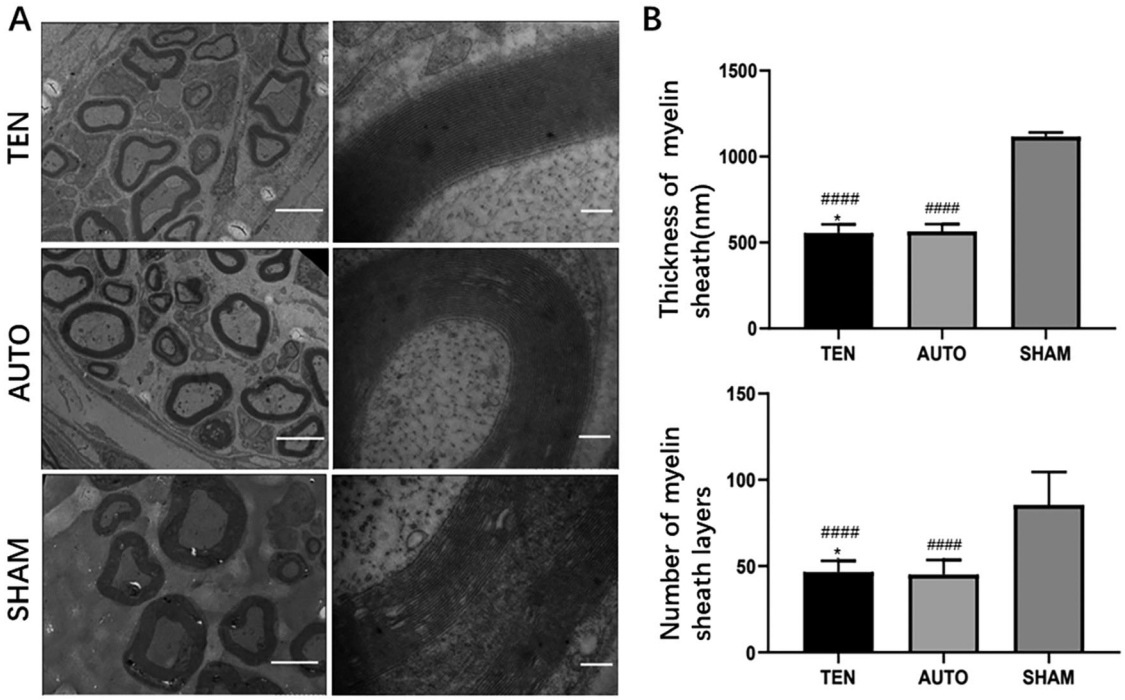

Figure 5. A) TEM images of transverse sections of the regenerated nerves, obtained at 12 weeks post-surgery; scale bars: 50 μm (left) and 0.2 μm (right). B) Histograms comparing the myelin sheath layers and myelin sheath thickness among groups. Data are expressed as mean ± SD, $n = 15$, one-way ANOVA was carried out across groups, *n.s. versus AUTO group and ####$p < 0.0001$ versus SHAM group.

2.7. Function Restoration

The results of the pain withdrawal threshold (PWT) and pain withdrawal response latency (PWL) measurements at 12 weeks post-operation showed that the TEN and AUTO groups did not differ significantly (**Figure 6**A). The electrophysiological study did not find a significant difference in the compound muscle action potential (CMAP) amplitudes and motor nerve conduction velocity values between the TEN and AUTO groups (Figure 6B,C). The behavioral assessments conducted using the CatWalk system showed that the sciatic nerve function index (SFI) results were consistent with the results of the electrophysiological analysis (Figure 6D,E).

2.8. Muscle Wet Weight Ratio and Degree of Fibrosis

12 weeks post-operation, the gastrocnemius muscles were trimmed and the ratio of wet weight between the operated and healthy sides was calculated (**Figure 7**A). Masson's trichrome staining analysis suggested that the area ratios of collagen fibers in the cross-sections of the gastrocnemius muscle belly were 13.235 ± 2.204%, 14.407 ± 5.483%, 6.657 ± 1.902%, and 28.505 ± 3.193%, in the TEN, AUTO, SHAM, and NON groups, respectively (Figure 7B). The wet weight ratio of the TEN group was similar to that of the AUTO group, both of which were higher than that of the NON group and lower than that of the SHAM group (Figure 7C). In terms of the degree of gastrocnemius fibrosis, there was no statistical difference between the TEN and AUTO groups, and both displayed a degree of gastrocnemius fibrosis that was lower than that of the NON group and higher than that of the SHAM group (Figure 7C).

3. Discussion

It is well known that using autogenous graft sources leads to the best histocompatibility, with minimal adverse reactions and relatively low implantation costs. However, the shortcomings of autologous nerve transplantation cannot be ignored.[4,6,5] The effect of TEN grafts in inducing distant axon regeneration and restoring sciatic nerve function may be similar to those of autografts, with even better clinical potential.[58–60] With progress in research, bionics have become the most important point of focus in nerve transplantation techniques.

Biodegradability is an important factor in tissue engineering. The degradation rate of chitosan can be determined by means of acetylation to adapt it to the speed of nerve regeneration.[26] Previous studies have shown that acetylated and pure chitosan scaffolds have similar effects in promoting nerve regeneration.[61] In the present study, chitin helical scaffolds were fabricated by means of mold casting and chitosan acetylation, and a fibrous membrane was electrospun on the outer layer of the chitin scaffold. Compared to traditional cylindrical scaffolds, there is a huge reduction in the amount of raw materials needed for TEN grafts, which reduces the risk of possible foreign body reactions and leads to faster degradation. In vivo degradation experiments showed that acetylated chitin degraded faster than chitosan and did not cause inflammatory responses. No second operation was needed, and transverse growth of the nerve was not hindered. The diameter of the new nerve was the same as that of the

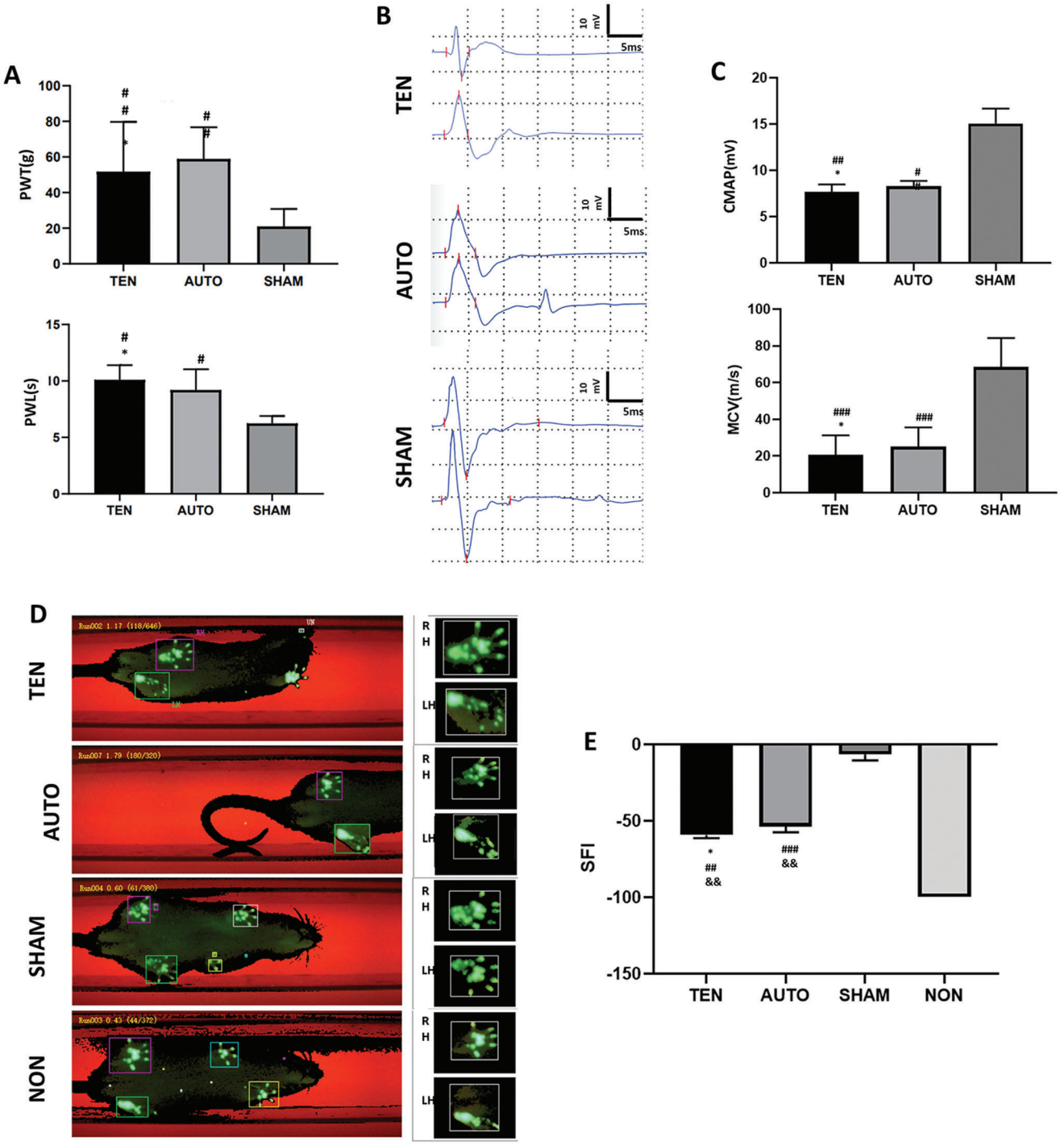

Figure 6. A) Histograms comparing the PWT and PWL of the injured side in the three groups obtained at 12 weeks post-operation. B) Representative CMAP recordings, with the traces recorded after stimulating the distal (upper traces) and proximal (lower traces) nerve portions. C) Histograms showing the CMAP amplitudes and MCV detected on the injured side of animals in the three groups. D) The footprints of the left (operated side) and right (healthy side) paws during walking. E) CatWalk gait analysis showing SFI values of the three experimental groups and controls at 12 weeks post-operation. Data are expressed as mean ± SD, $n = 12$, one-way ANOVA was carried out across groups, *n.s. versus AUTO group, #$p < 0.05$ versus SHAM group, ##$p <$ 0.01 versus SHAM group, ###$p < 0.001$ versus SHAM group, and &&$p < 0.01$ versus NON group.

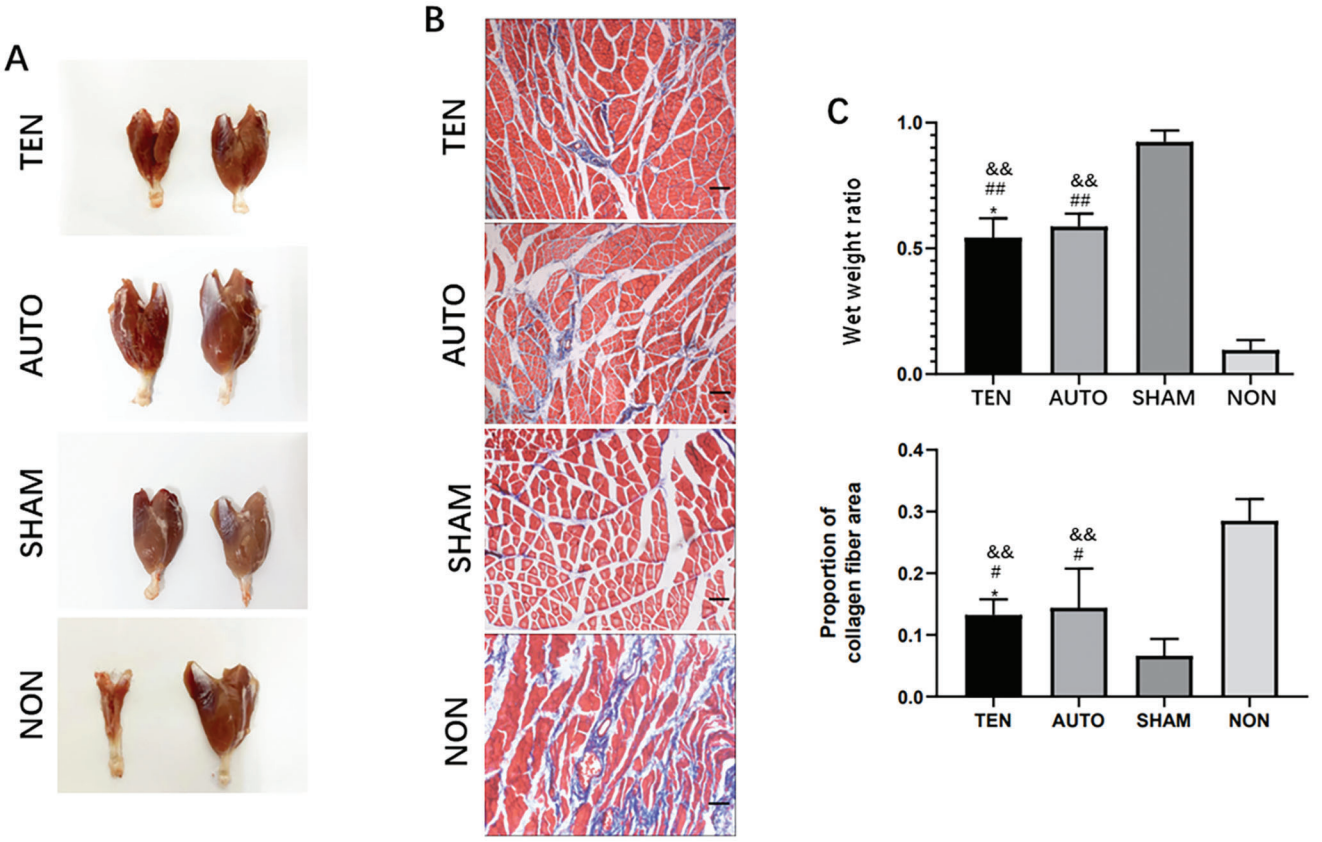

Figure 7. A) Gastrocnemius muscles obtained at 12 weeks post-operation from the operated (left) and healthy (right) sides. B) Masson's trichrome staining of the gastrocnemius samples; muscle fibers are in red, while collagen fibers are in blue; Scale bar: 10 μm. C) Histograms of the wet weight ratios of the gastrocnemius and the average cross-sectional areas of the muscle fibers at 12 weeks post-operation. Data are expressed as mean ± SD, $n = 15$, one-way ANOVA was carried out across groups, *n.s. versus AUTO group, #$p < 0.05$ versus SHAM group, ##$p < 0.01$ versus SHAM group, and &&$p < 0.01$ versus NON group.

residual nerve at both ends (Figure 3F). On the other hand, a scaffold with a non-degradable or slow degradation rate would limit the lateral growth of regenerated nerves.[62] The outer electrospun chitosan film could meet the conditions for liquid exchange inside and outside the TEN graft, and the average pore size was much smaller than that of fibroblasts and inflammatory cells. The special structure not only ensured the exchange of matter, but also prevented the invasion of connective tissue and the growth of new neurofilaments out of the scaffold in the wrong direction. The WCA of each structural layer of the TEN grafts showed that they were hydrophilic (WCA < 90°), which is beneficial for nutrient exchange and cell adhesion. Several studies in the literature have shown that under the same conditions, the nerve repair effect of the naked cylindrical scaffold is not as good as that of the scaffold with an internal guidance design.[63] Our research group has also verified this conclusion and showed that the inner fiber plays an indispensable role.[64] Fibers with a unique T-shaped cross-section can be used as a topographic guide to make Schwann cells migrate directionally and mediate the directional growth of proximal new nerve fibers to the distal end with the highest efficiency. Moreover, compared to the ordinary smooth filamentary structure, the filaments of this special T-shaped cross-sectional structure can be gathered into bundles that are not tightly attached and leave gaps between each other owing to the lateral protrusions, thereby providing space and active terrain guidance for nerve growth. Cytotoxicity and hemolysis are important components in the evaluation of material biocompatibility, and constitute basic conditions for tissue engineering candidate materials. The classical theory of tissue engineering involves three elements: biomaterials, seed cells, and factors.[65,66] Replacing the seed cells and factor components added to the scaffold with hBMSC-dECM resulted in the successful preparation of the TEN grafts. The repair effects of these grafts were then tested on rat sciatic nerves with 10-mm defects, which are currently the most commonly studied defect length and can be classified as long-distance defects, as compared to 3- or 5-mm ones.[67–69]

Although many studies have shown that different nerve scaffolds can successfully repair nerve injury in rats, the speed and effect of repair were uneven and statistically different from those of autogenous nerve transplantation.[70,71] Therefore, in this study, histological and functional evaluations were performed after nerve transplantation, with an emphasis on the comparison of regeneration effects between the TEN and AUTO groups. Anti-

NF-200 immunohistochemical staining showed that 3 weeks after the operation, the regenerated nerve fibers in the TEN group connected the distal nerve through the scaffolds, and labeling of the neural stem cell and Schwann cell markers NF200 and S100β was observed at 8 weeks after transplantation. Axon densities of the distal regenerated nerves were also compared. The effects of nerve repair were similar between the TEN and AUTO groups. Morphological observations and analysis of nerve fibers in the surgical group showed that the TEN group promoted the formation of the myelin sheath, with effects similar to those in the AUTO group.

One of the main nerves innervating the hindlimbs, the sciatic nerve, is particularly responsible for foot movement and proprioception. The PWT and PWL were used to evaluate sensory function recovery, while electrophysiology and gait analysis were used to evaluate motor function recovery. The PWT and PWL showed similar results in the TEN and AUTO groups. The motor nerve conduction velocity and CMAP in the TEN implantation area provided information on the nerve impulse conduction and degree of myelin regeneration of the newly grown nerve, respectively. The TEN group showed functional recovery accompanied by peripheral nerve regeneration, and the effects were not significantly different from those of AUTO treatment. However, the low CMAP values in the TEN and AUTO groups are likely attributable to myelin loss and incomplete nerve regeneration caused by persistent axonal injury. These results suggested that the TEN group was similar to the AUTO group in terms of promotion of sensory and motor function recovery. To date, most studies have reported an average regeneration duration of 3–4 months until the growth of a new nerve along the canal that completely filled the gap. However, nerve regeneration is a very complex and slow process,[72] and functional recovery is not necessarily related to the number of axons in the regenerated body;[73,74] therefore, it takes longer to recover strength and sensory functions.[75] Owing to this, future studies should include longer follow-up periods to fully compare functional recovery.

The structure, function, and nutrition of the skeletal muscles depend on the innervating peripheral nerves. Skeletal muscle fibers undergo rapid atrophy after denervation, with shrinkage in muscle volume and loss of contractile function. After longer periods of denervation, muscle fiber atrophy is further aggravated and gradually replaced by hyperplastic connective and adipose tissues; this is the process of muscle fibrosis.[76] Therefore, we evaluated peripheral nerve repair in terms of the degree of atrophy and fibrosis of the target muscle. We compared the wet weight ratios and degrees of gastrocnemius fibrosis using Masson's staining. This conclusion was consistent with the results of the morphological and functional experiments described above.

In summary, a novel bionic TEN grafting method for repairing peripheral nerve injury was designed and used to connect a 10-mm sciatic defect in rats. The effect of this method in nerve regeneration was similar to that of the autografts. The method described herein improves upon the previous TEN methods, by fully simulating peripheral nerves in composition and structure and achieving more ideal repair effects, similar to those obtained using autogenous nerves. Therefore, this study offers a potential novel choice for clinical applications.

4. Conclusions

This study proposes a new way to develop bionic TEN grafts with advantageous bionic structure and composition. When used to connect a 10-mm sciatic defect in rats, the TEN grafts showed good supporting effects on myelin formation, axonal growth, and sensory and motor recovery, similar to those displayed by autografts. The novel bionic TEN graft described in this study can be directly carried forward to future peripheral nerve injury clinical trials.

5. Experimental Section

Isolation and Characterization of hBMSC-dECM: hBMSCs were purchased and passaged in special medium, according to the manufacturer's instructions (Biological Industries, Israel). When the cell density reached 80%, ascorbic acid (50 μg mL^{-1}; Sigma-Aldrich, St. Louis, MO, USA) was used to stimulate ECM production. For decellularization after culturing for 10 d, the cell cultures were incubated with Milli-Q water at 37 °C for 10 min and treated with 3% (v/v) Triton X-100 plus 2% sodium dodecyl sulfate (Sigma-Aldrich), at 37 °C for 5 min, and 100 U mL^{-1} DNase I (Invitrogen, Carlsbad, CA, USA), for 2 h. The main components were then characterized using immunohistochemistry. DNA was extracted from the cells using a mammalian genomic DNA extraction kit (Beyotime, Shanghai, China).

TEN Graft Fabrication: For the specific process of TEN graft fabrication, please refer to the patent form (patent application no. CN202211269678.0) submitted by our team. Chitosan was dissolved in 2% acetic acid to obtain a 6% chitosan solution. The solution was spread evenly on a helical rod-shaped mold with an outer diameter of 2 mm, cured with 5% sodium hydroxide for 12 h, and washed to neutral pH. The product was freeze-dried and the outer layer of chitosan was carefully removed to obtain a helical scaffold that was trimmed to a length of 12 mm to leave a 10 mm gap after connecting the end of the nerve. Each helical scaffold (0.2 g) was acetylated with methanol/acetic anhydride solution (150 mL) for 6 h, solidified with 10% sodium hydroxide for 12 h, washed to neutral pH, and dried to obtain a helical chitin scaffold. After electrospinning for 3 h in the mode of uniform translation of the nozzle, 4% chitosan fiber membranes were uniformly wrapped around the outside of the helical scaffold. The chitosan/hBMSCs-dECM-mixed fibers were fabricated on a polydimethylsiloxane (PDMS) mold with T-shaped fine filamentous grooves using vacuum- and freeze-drying technology. The fibers were then trimmed to a length of 20 mm to be used as inner fibers to be fixed at both ends of the scaffold with surgical sutures and kept horizontal. Five inner fibers were used for each scaffold. The hBMSC-dECMs obtained, as described in section 5.1, were directly wrapped on the outside of the fibers and inserted into the scaffold together. All hBMSC-dECM samples obtained from a large cell Petri dish at the same passage number, cell density, and culture method were used in each scaffold. As mentioned above, a novel bionic TEN graft was constructed using a chitin helical scaffold as the supporting structure, hBMSC-dECM as nutrients, and chitosan/hBMSC-dECM inner fibers as a terrain guide (**Figure 8**).

TEN Characterization: The morphology of the outermost electrospun membranes and fibers was observed using a SEM (Hitachi S-3400 NII, Japan), and the images thus obtained were analyzed using ImageJ software[77] to study the fiber porosity and average pore size. FTIR spectra of the scaffolds before and after acetylation were recorded using a Nicolet IS 50 spectrometer (Thermo Fisher Scientific, Waltham, MA, USA). The WCA of each layer was measured using a contact angle apparatus (Dedu, JY-Pha, China).

Cell Viability and Hemolysis Assays: The TEN graft was immersed in Dulbecco's modified Eagle medium (Thermo Fisher Scientific), to obtain the extraction medium samples. L929 cells were selected according to the national standard of the People's Republic of China (GB/T 16886.5-1997-ISO 10993–5RU 1992) and cultured with extracts obtained from the TEN

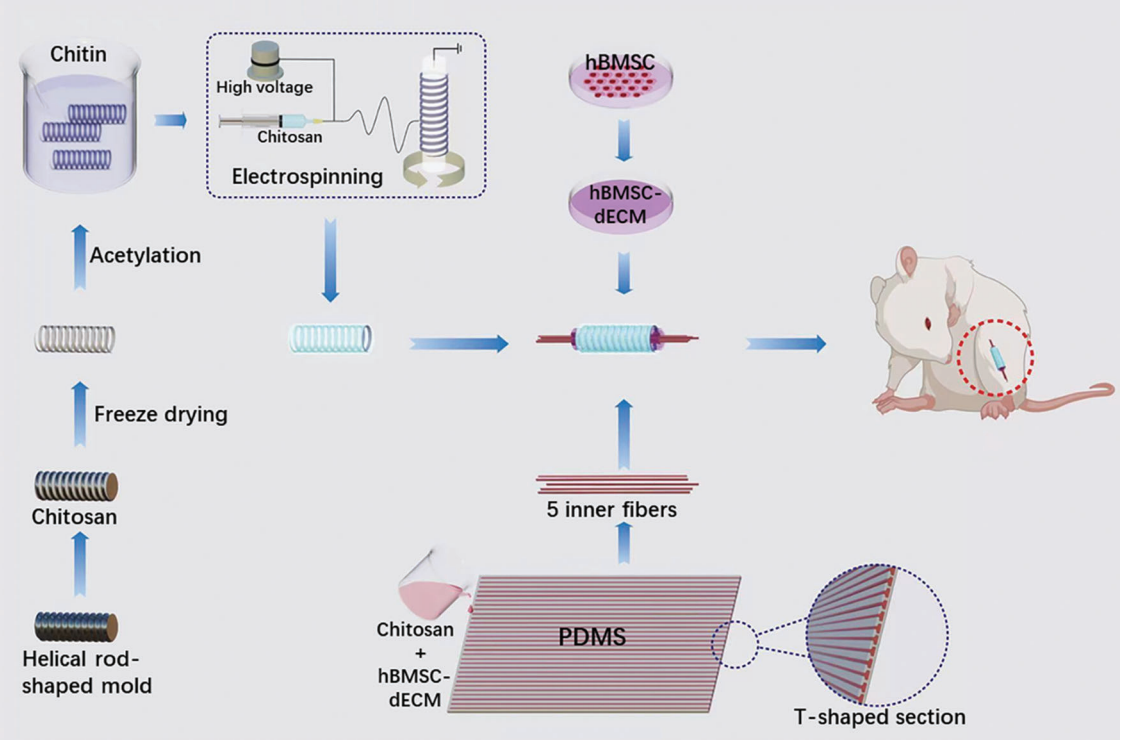

Figure 8. Schematic representation of the TEN graft production.

grafts. Dulbecco's modified Eagle medium alone was used as a control in this experiment. The effects of the TEN graft on L929 cytotoxicity were assessed using an MTT assay (Beyotime). A mini tablet reader (BioTek, Winooski, VT, USA) was used to record the absorbance at 570 nm.

Fresh rabbit blood was obtained according to the national standard GB/T16886.1-1997-ISO 10993–4 of the People's Republic of China, collected in a tube with heparin, and diluted with normal saline. A suspension of the TEN graft materials at a concentration of 5 mg mL^{-1} was prepared in normal saline. Diluted blood (100 µL) was added to 5 mL of the TEN graft suspension, saline, and distilled water. After incubation at 37 °C and centrifugation, the absorbance was measured at 545 nm. The hemolysis rate (%) was calculated as follows:

$$\text{Hemolysis ratio} = \frac{\text{Dt} - \text{Dnc}}{\text{Dpc} - \text{Dnc}} \times 100\% \quad (1)$$

where Dt is the absorbance of the TEN group, Dnc is the absorbance of the saline group, and Dpc is the absorbance of the distilled water group.

In Vitro and In Vivo Degradation: The degradation rates of the samples before and after acetylation were evaluated using enzymatic degradation in vitro. The samples were immersed in a 0.3% pancreatin solution made in phosphate-buffered saline (Sigma-Aldrich). Experiments were conducted at 37 °C and the enzyme medium was changed every 48 h. Samples were collected at scheduled times, washed with distilled water, dried, and weighed. The following equation was used to calculate weightlessness ratio:

$$\text{Weightlessness ratio} = \frac{\text{Initial weight} - \text{Remaining weight}}{\text{Initial weight}} \times 100\% \quad (2)$$

In vivo experiments were conducted on the backs of rats. Freeze-dried samples were cut into 10 × 10 mm slices, disinfected with high-pressure steam, and dried. The different sample groups were buried on different sides of the backs of the rats. The samples and surrounding tissues were removed at scheduled times for paraffin sectioning. According to the manufacturer's instructions, a H&E Staining Kit (Beyotime) was used, and the morphology of the material and inflammatory reactions of the surrounding tissue were observed using a Zeiss Axio Imager M2 (Carl Zeiss AG, Oberkochen, German). At the same time, some samples were soaked in collagenase and Triton X-100 to remove the surrounding tissue and then observed using SEM.

Animal Surgery: Sprague-Dawley rats weighing 180–200 g were provided by the Experimental Animal Center of Nantong University (Jiangsu, China). All experiments involving animals were performed in accordance with Institutional Animal Care guidelines and approved ethically by the Administration Committee of Experimental Animals, Jiangsu Province, China (approval no: S20210309-009).

The sciatic nerve was exposed after an intraperitoneal injection of a compound anesthetic (4 mL kg^{-1} body weight). The sciatic nerve was excised, leaving a 10 mm gap after the nerve endings were retracted. The animals were divided into four groups: bionic TEN (TEN), autogenous nerve (AUTO), sham operation (SHAM), and non-grafted (NON). The 10 mm defect was bridged according to the group assignment. After the operation, the animals were kept in a standard manner, observed regularly, and evaluated using histomorphology and functional tests.

Immunocytochemistry and Immunohistochemistry: The hBMSC-dECM specimens were incubated with the following primary antibodies: mouse polyclonal antibody against fibronectin (1:500; ab154210, Abcam, Cambridge, UK), rabbit polyclonal antibody against collagen I (1:250; ab260043, Abcam), and rat polyclonal antibody against laminin (1:10; ab2466, Abcam). This was followed by incubation with fluorescently labeled secondary antibodies: goat anti-rat IgG(H+L) (Alexa Fluor 647) (1:500; ab150167, Abcam), Cy3-conjugated affinipure goat anti-rabbit IgG(H+L) (1:50; SA000092, Proteintech, Chicago, US), and CoraLite 488-conjugated goat anti-mouse IgG(H+L) (1:300; SA000013, Proteintech). Antifade Mounting Medium with Hoechst (Beyotime) was used to seal and preserve the film.

After 3 and 8 weeks, the nerve tissue specimens were incubated with the following primary antibodies: rabbit anti-S100β polyclonal antibody (1:100; ab52642, Abcam) and mouse anti-NF200 monoclonal anti-

body (1:50; N5389, Sigma-Alrdich, Darmstadt, German) followed by secondary antibodies: donkey anti-rabbit IgG(H+L) (Alexa Fluor 488) (1:500; ab150073, Abcam) and goat anti-mouse IgG(H+L) (Alexa Fluor 594) (1:500; ab150120, Abcam). Next, Zeiss Axio Imager M2 was used to image samples and ImageJ software was used to analyze the images.

TEM: 12 weeks after the operation, the distal ends of the regenerated nerve specimens were prepared and observed using TEM (HT7700, JEOL Ltd., Tokyo, Japan).[78] ImageJ software was used to calculate the myelin thickness and myelin layers.

CatWalk Gait Analysis and Electrophysiological Assessment: The CatWalk XT 9.0 (Noldus, Wageningen, Netherlands) Gait Analysis System was used to assess motor functional recovery at 12 weeks post-operation. The SFI was calculated and ranged from −100 to 0, with −100 indicating complete hindlimb paralysis and 0 indicating normal function. The Bain formula was used to calculate the SFI value:

$$\mathrm{SFI} = \frac{109.5\ (\mathrm{ETS} - \mathrm{NTS})}{\mathrm{NTS}} - \frac{38.3\ (\mathrm{EPL} - \mathrm{NPL})}{\mathrm{NPL}} + \frac{13.3\ (\mathrm{EIT} - \mathrm{NIT})}{\mathrm{NIT}} - 8.8 \quad (3)$$

where TS is toe expansion, PL is print length, IT is middle toe expansion, and E and N are experimental and normal contralateral hind foot, respectively.

Electrophysiological tests were performed at 12 weeks post-operation. In short, the sciatic nerve was contacted again on the surgical side under anesthesia, and the far and near nerve endings were stimulated with an electric current of 10 mA using a portable digital MYTO electrophoresis and Galileo NT system software (Esaote, Genoa, Italy), following which the CMAPs were recorded. Motor nerve conduction velocity was determined by dividing the distance between two trigger points by the CMAP senses at the two trigger points.

Mechanical and Thermal Pain Threshold Measurement: To evaluate the recovery of sensory function, the mechanical PWT and thermal PWL of the rats were measured at 12 weeks post-operation. Von Frey filaments (Stoelting, Wood Dale, IL, USA) were used to stimulate the sole of the operated foot for 2–3 s; three such stimulations were carried out with an interval of 10 s. Shrinking and foot-licking behaviors showed positive functional recovery. The up-and-down method was used, and the PWT was calculated.[79] The PWL on the operative side of the rats was measured using the Hargreaves test and a thermal pain tester (390G; IITC Life Science Inc., Woodland Hills, CA, USA).[79] The infrared radiation heat source was placed in the middle of the plantar surface on the operative side. The average value of the three tests was recorded as the PWL, with an interval of 5 min between the tests.

Muscle Wet Weight Ratio and Degree of Fibrosis: The wet weight ratio was measured at 12 weeks post-operation (operative side weight/healthy side weight), after removing and weighing the gastrocnemius muscle. The gastrocnemius muscles were used to prepare paraffin sections. According to the manufacturer's instructions, muscle and collagen fibers were stained using a Modified Masson's Trichrome Stain Kit (Solarbio Life Science, Beijing, China), and the proportion of collagen fibers was counted on microscope images using ImageJ software.

Statistical Analysis: Data are presented as mean ± standard deviation. The Student's *t*-test was used to compare two samples, and the one-way ANOVA with Fisher LDS test was used for the comparison between multiple groups. Prism (GraphPad Software Inc., San Diego, CA, USA) was used for statistical analysis, and statistical significance was set at $p < 0.05$.

Ethics Approval Statement: The work described herein is original research that has not been published previously and is not under consideration for publication elsewhere, in whole or in part. All the authors listed have approved the enclosed manuscript.

Acknowledgements

This work was supported by the National Natural Science Foundation of China (grant no. 32130060) and the Natural Science Foundation of Jiangsu Province (grant no. BK20202013).

Conflict of Interest

The authors declare no conflict of interest.

Data Availability Statement

The data that support the findings of this study are available on request from the corresponding author. The data are not publicly available due to privacy or ethical restrictions.

Keywords

bionic tissue engineering, extracellular matrix, helix scaffolds, nerve regeneration

Received: December 8, 2022
Revised: February 15, 2023
Published online: March 22, 2023

[1] H. Millesi, *Hand Clin.* **2000**, *16*, 73.
[2] D. Grinsell, C. P. Keating, *J. Biomed. Biotechnol.* **2014**, *2014*, 698256.
[3] M. Samii, *Langenbecks Arch. Chir.* **1972**, *332*, 355.
[4] X. Gu, F. Ding, Y. Yang, L. Jie, *Prog. Neurobiol.* **2011**, *93*, 204.
[5] M. Idini, P. Wieringa, S. Rocchiccioli, G. Nieddu, L. Moroni, *Acta Biomater.* **2019**, *96*, 188.
[6] N. B. Fadia, J. M. Bliley, G. A. Dibernardo, D. J. Crammond, K. G. Marra, *Sci. Transl. Med.* **2020**, *12*, eaav7753.
[7] A. Atala, S. B. Bauer, S. Saker, J. J. Yoo, A. B. Retik, *J. Urol.* **2007**, *177*, 66.
[8] J. Tao, J. Zhang, T. Du, X. Xu, X. Deng, S. Chen, J. Liu, Y. Chen, X. Liu, M. Xiong, *Acta Biomater.* **2019**, *90*, 49.
[9] M. Georgiou, J. P. Golding, A. J. Loughlin, P. J. Kingham, J. B. Phillips, *Biomaterials* **2015**, *37*, 242.
[10] Z. Zhang, M. L. Jrgensen, Z. Wang, J. Amagat, M. Chen, *Biomaterials* **2020**, *253*, 120108.
[11] C. R. Carvalho, J. M. Oliveira, L. R. Rui, *Front. Bioeng. Biotechnol.* **2019**, *7*, 337.
[12] C. Hinüber, K. Chwalek, F. J. Pan-Montojo, M. Nitschke, R. Vogel, H. Brünig, G. Heinrich, C. Werner, *Acta Biomater.* **2014**, *10*, 2086.
[13] T. Hadlock, C. Sundback, D. Hunter, M. Cheney, J. P. Vacanti, *Tissue Eng.* **2000**, *6*, 119.
[14] W. W. Ashley, T. Weatherly, T. S. Park, *J. Neurosurg. Case Lessons* **2006**, *105*, 452.
[15] B. D. Bushnell, A. D. Mcwilliams, G. B. Whitener, T. M. Messer, *J. Hand Surg. Am.* **2008**, *33*, 1081.
[16] R. Deumens, A. Bozkurt, M. F. Meek, M. A. E. Marcus, G. A. Brook, *Prog. Neurobiol.* **2010**, *92*, 245.
[17] O. S. Manoukian, J. T. Baker, S. Rudraiah, M. R. Arul, S. G. Kumbar, *J. Controlled Release* **2019**, *317*, 78.
[18] T. Freier, S. K. Hui, K. Kazazian, M. S. Shoichet, *Biomaterials* **2005**, *26*, 5872.
[19] K. Haastert-Talini, S. Geuna, L. B. Dahlin, C. Meyer, L. Stenberg, T. Freier, C. Heimann, C. Barwig, L. F. V. Pinto, S. Raimondo, G. Gambarotta, S. R. Samy, N. Sousa, A. J. Salgado, A. Ratzka, S. Wrobel, C. Grothe, **2013**, *34*, 9886.
[20] Y. Ying, P. Zhang, Y. Yang, X. Wang, X. Gu, *Biomaterials* **2004**, *25*, 4273.
[21] M. J. Simões, A. Gärtner, Y. Shirosaki, R. M. G. D. Costa, A. C. Maurício, *Acta Med. Port.* **2011**, *24*, 43.
[22] L. Huang, X. Yang, L. Deng, D. Ying, B. Duan, *ACS Appl. Mater. Interfaces.* **2021**, *13*, 16106.
[23] N. Florian, S. Michael, M. Wibke, S. Jessica, H. Sina, H. Leila, B. Berthold, K. Ulrich, K. Thomas, *Plast. Reconstr. Surg.* **2018**, *142*, 415.

[24] Y. Gong, L. Gong, X. Gu, D. Fei, *Microsurgery* **2010**, *29*, 650.
[25] Y. M. Yang, W. Hu, X. D. Wang, X. S. Gu, *J. Mater. Sci.: Mater. Med.* **2007**, *18*, 2117.
[26] I. Younes, M. Rinaudo, *Mar. Drugs* **2015**, *13*, 1133.
[27] M. Tsurkan, A. S. Voronkina, Y. Khrunyk, M. Wysokowski, H. Ehrlich, *Carbohydr. Polym.* **2020**, *252*, 117204.
[28] A. C. A. Wan, B. C. U. Tai, *Biotechnol. Adv.* **2013**, *31*, 1776.
[29] T. Freiera, R. Montenegroc, S. K. Hui, M. S. Shoicheta, *Biomaterials* **2005**, *26*, 4624.
[30] B. Sva, *Acta Biomater.* **2020**, *106*, 54.
[31] H. Lu, T. Hoshiba, N. Kawazoe, I. Koda, M. Song, G. Chen, *Biomaterials* **2011**, *32*, 9658.
[32] D. Sharma, M. Ferguson, F. Zhao, *Methods Cell Biol.* **2020**, *156*, 3.
[33] M. Winterbottom, *Rev. Neurosci.* **2013**, *24*, 443.
[34] X. Zhang, X. Chen, H. Hong, R. Hu, J. Liu, C. Liu, *Bioact. Mater.* **2022**, *10*, 15.
[35] S. Wang, C. Zhu, B. Zhang, J. Hu, J. Xu, C. Xue, S. Bao, X. Gu, F. Ding, Y. Yang, *Biomaterials* **2021**, *280*.
[36] J. A. Lohmeyer, S. Zimmermann, B. Sommer, H. G. Machens, P. Mailnder, *Chirurg* **2007**, *78*, 142.
[37] F. Stang, H. Fansa, G. Wolf, M. Reppin, G. Keilhoff, *Biomaterials* **2005**, *26*, 3083.
[38] O. Alluin, C. Wittmann, T. Marqueste, J. F. Chabas, S. Garcia, M. N. Lavaut, D. Guinard, F. Feron, P. Decherchi, *Biomaterials* **2009**, *30*, 363.
[39] A. Mobasseri, A. Faroni, B. M. Minogue, S. Downes, G. Terenghi, A. J. Reid, *Tissue Eng., Part A* **2015**, *21*, 1152.
[40] D. Sven, D. Lutz, B. Peter, W. Soenke, C. Tanmay, *Biomed Res. Int.* **2014**, *2014*, 835269.
[41] R. Foltán, K. Klíma, J. Spacková, J. Sedý, *Med. Hypotheses* **2008**, *71*, 572.
[42] T. Gros, J. S. Sakamoto, A. Blesch, L. A. Havton, M. H. Tuszynski, *Biomaterials* **2010**, *31*, 6719.
[43] S. Stokols, J. Sakamoto, C. Breckon, T. Holt, M. H. Tuszynski, *Tissue Eng.* **2006**, *12*, 2777.
[44] D. Hoffman-Kim, J. A. Mitchel, R. V. Bellamkonda, *Annu. Rev. Biomed. Eng.* **2010**, *12*, 203.
[45] D. N. Brooks, R. V. Weber, J. D. Chao, B. D. Rinker, J. Zoldos, M. R. Robichaux, S. B. Ruggeri, K. A. Anderson, E. E. Bonatz, S. M. Wisotsky, M. S. Cho, C. Wilson, E. O. Cooper, J. V. Ingari, B. Safa, B. M. Parett, G. M. Buncke, *Microsurgery* **2012**, *32*, 1.
[46] M. F. Meek, J. P. A. Nicolai, P. H. Robinson, *J. Reconstr. Microsurg.* **2006**, *22*, 149.
[47] Y.-G. Zhang, Q.-S. Sheng, F.-Y. Qi, X.-Y. Hu, W. Zhao, Y.-Q. Wang, L.-F. Lan, J.-H. Huang, Z.-J. Luo, *J. Mater. Sci. Mater. Med.* **2013**, *24*, 1767.
[48] A. Bozkurt, F. Lassner, O. Dan, R. Deumens, A. Bcker, T. Schwendt, C. Janzen, C. V. Suschek, R. Tolba, E. Kobayashi, *Biomaterials* **2012**, *33*, 1363.
[49] K. Sachiro, N. Midori, M. Toshiyuki, Y. Tetsuji, *Front. Chem.* **2014**, *2*, 00052.
[50] H. Cao, T. Liu, S. Y. Chew, *Adv. Drug Deliv. Rev.* **2009**, *61*, 1055.
[51] B. S. Jha, R. J. Colello, J. R. Bowman, S. A. Sell, K. D. Lee, J. W. Bigbee, G. L. Bowlin, W. N. Chow, B. E. Mathern, D. G. Simpson, *Acta Biomater.* **2011**, *7*, 203.
[52] A. Yw, Y. B. Zhou, A. Kl, A. Jh, *Appl. Surf. Sci. 501*, 144279.
[53] A. Sjp, B. Bkl, A. Mhn, A. Dsk, *Acta Biomater.* **2013**, *9*, 7719.
[54] S. Mahalingam, R. Matharu, S. Homer-Vanniasinkam, M. Edirisinghe, *Appl. Phys. Rev.* **2020**, *7*, 041302.
[55] K. Chwalek, Y. Dening, C. Hinueber, H. Bruenig, M. Nitschke, C. Werner, *Mater. Sci. Eng., C* **2016**, *61*, 466.
[56] G. Xupeng, W. Yu, C. Jifeng, P. Jiang, *Rev. Neurosci.* **2013**, *24*, 0022.
[57] S. Beil, A. Schamberger, W. Naumann, S. Machill, K. Pée, *Carbohydr. Polym.* **2012**, *87*, 117.
[58] A. Ivy, B. Bjh, *Biomaterials* **2004**, *25*, 1593.
[59] M. Rosewich, S. Adler, S. Zielen, *J. Reconstr. Microsurg.* **2001**, *17*, 589.
[60] M. F. Meek, W. F. A. D. Dunnen, J. M. Schakenraad, P. H. Robinson, *Microsurgery* **1996**, *17*, 555.
[61] K. Haastert-Talini, S. Geuna, L. B. Dahlin, C. Meyer, L. Stenberg, T. Freier, C. Heimann, C. Barwig, L. F. V. Pinto, S. Raimondo, G. Gambarotta, S. R. Samy, N. Sousa, A. J. Salgado, A. Ratzka, S. Wrobel, C. Grothe, *Biomaterials* **2013**, *34*, 9886.
[62] B. Z. Sun, Z. F. Wu, T. Chen, W. M. Li, D. W. Zheng, H. El-Hamshary, H. Al-Deyab, S. S. Mo, X. M. Ye, Y. X, *ACS Appl. Mater. Interfaces* **2017**, *9*, 26684.
[63] S. Kbl, *Int. J. Mol. Sci.* **2022**, *23*, 1244.
[64] P. Lu, G. Wang, T. Qian, X. Cai, P. Zhang, M. Li, Y. Shen, C. Xue, H. Wang, *Mater. Today Bio* **2021**, *12*, 100158.
[65] S. Yi, L. Xu, X. Gu, *Exp. Neurol.* **2018**, *319*, 112761.
[66] Z. Pei-Xun, H. Na, K. Yu-Hui, Z. Qing-Tang, L. Xiao-Lin, *Neural Regen. Res.* **2019**, *14*, 51.
[67] Y. Hu, Z. Chen, H. Wang, J. Guo, J. Cai, X. Chen, H. Wei, J. Qi, Q. Wang, H. Liu, *ACS Nano* **2022**, *16*, 1868.
[68] Y. Zhang, H. Luo, Z. Zhang, Y. Lu, X. Huang, Y. Lu, J. Xu, Y. Wei, X. Fan, B. Du, *Biomaterials* **2010**, *31*, 5312.
[69] D. Mei, S. Bo, D. Liu, J. H. Liu, Q. D. Shen, *ACS Nano* **2020**, *14*, 5135.
[70] A. Gopinath, R. Thangam, S. Perumal, D. Masilamani, S. K. Ramadass, B. Madhan, *Mater. Sci. Eng., C.* **2018**, *92*, 297.
[71] A. Thibodeau, T. Galbraith, C. M. Fauvel, H. T. Khuong, F. Berthod, *Biomaterials* **2022**, *280*, 121269.
[72] M. Boeckstyns, S.-A. I. Rensen, V.-J. F. Eta, B. Rosén, X. Navarro, S. J. Archibald, J. Valss-Solé, M. Moldovan, C. Krarup, *J. Hand Surg. Eur. Vol.* **2013**, *38*, 2405.
[73] S. Neerven, A. Bozkurt, *J. Brachial Plex. Peripher. Nerve Inj.* **2012**, *7*, 5.
[74] M. Wood, S. Kemp, C. Weber, G. H. Borschel, T. Gordon, *Ann. Anat.* **2011**, *193*, 321.
[75] S. Das, M. Sharma, K. Sarma, B. Konwar, B. Bibhuti, *Biomaterials* **2015**, *62*, 66.
[76] M. Siemionow, T. G. Brzezicki, *Int. Rev. Neurobiol.* **2009**, *87*, 141.
[77] B. Davis, M. Schwartz, D. Duchemin, J. Carl Barrett, G. Post, J. J. Wang, Z. Y. Xumonette, K. J. Jabbar, Q. Shen, G. C. Manyam, NIH Image to ImageJ: 25 years of image analysis, **2017**.
[78] X. Wang, W. Hu, Y. Cao, J. Yao, J. Wu, X. Gu, *Brain* **2005**, *128*, 1897.
[79] F. W. Stahnisch, *Sudhoffs Arch.* **2018**, *98*, 182.